

Electronic Supplementary Information (ESI)

Synergistic Effects of Copolymerization and Fluorination on Acceptor Polymers for Efficient and Stable All-Polymer Solar Cells

Nan Zhang, Yunxiang Xu, Xiaobo Zhou, Wei Zhang,* Ke Zhou, Liangmin Yu, Wei Ma,* & Xiaofeng Xu,*

Table of Contents

1. Materials.....	S2
2. Polymerization	S2
3. Thermogravimetric analysis (TGA) measurements	S4
4. Optical properties	S5
5. Electrochemical properties	S6
6. $J-V$ and EQE characteristics of the conventional and inverted all-PSCs	S7
7. $J-V$ and EQE characteristics of the all-PSCs with different D:A ratio.....	S9
8. $J-V$ characteristics of the all-PSCs with different thermal annealing.....	S10
9. $J-V$ characteristics of the all-PSCs with different solvent additives.....	S11
10. $J-V$ characteristics of the all-PSCs with different active areas	S13
11. $J-V$ and EQE characteristics of the thick-film all-PSCs	S14
12. Tapping-mode atomic force microscopy (AFM) images	S15
13. Grazing incidence wide-angle X-ray scattering (GIWAXS) measurements	S16
14. Relative dielectric constants measurements	S17
15. Time resolved photoluminescence (TRPL) measurements.....	S17
16. Space charge limited current (SCLC) mobility measurements	S19
17. Recombination characterization.....	S21
18. Thermal stability of the all-PSCs	S21
19. Transmittance of the substrates	S22
20. $J-V$ characteristics of the flexible all-PSCs	S22
21. Reference.....	S24

1. Materials

All reactions involving air-sensitive reagents were performed under a nitrogen atmosphere. The monomers 2,6-dibromonaphthalene-1,4,5,8-tetracarboxylic-*N,N'*-bis(2-octyldodecyl)diimide (NDIBr_2),^{1,2} 5,5'-bis(trimethylstannyl)-2,2'-bithiophene (2T) and 2,5-bis(trimethylstannyl)-3,4-difluorothiophene (TF)^{3,4} were synthesized following literature reports.

Poly[(2,6-(4,8-bis(5-(2-ethylhexyl)thiophen-2-yl)-benzo[1,2-*b*:4,5-*b'*]dithiophene))-alt-(5,5-(1',3'-di-2-thienyl-5',7'-bis(2-ethylhexyl)benzo[1',2'-*c*:4',5'-*c'*]dithiophene-4,8-dione)] (PBDB-T)^{5,6} and Poly[[*N,N'*-bis(2-hexyldecyl)naphthalene-1,4,5,8-bis(dicarboximide)-2,6-diyl]-*alt*-5,5'-(2,2'-bithiophene)] (N2200)⁷ were prepared according to the previous reports.

2. Polymerization

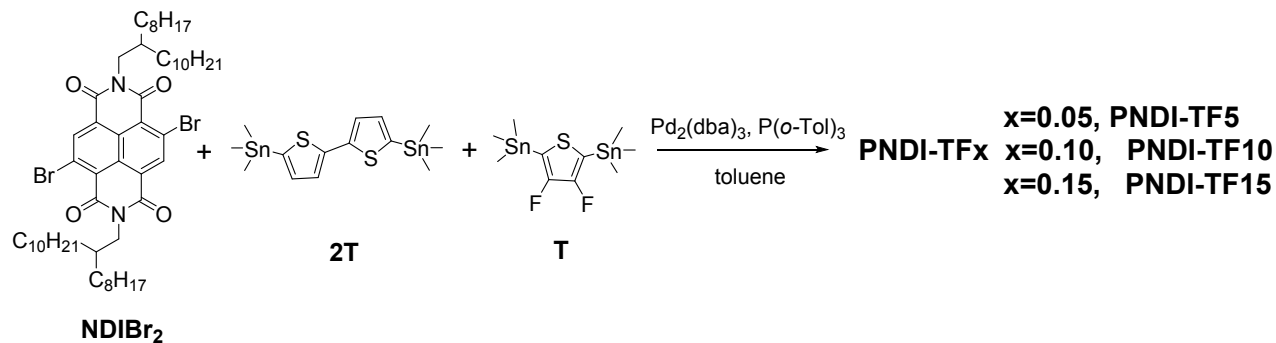


Figure S1. A synthetic route of the polymers PNDI-TFx.

General Procedure

The dibromo-substituted monomer (0.25 mmol), the bis(trimethylstannyl)-substituted monomer (0.25 mmol), tris(dibenzylideneacetone)dipalladium(0) ($\text{Pd}_2(\text{dba})_3$) (4.58 mg) and tri(*o*-tolyl)phosphine ($\text{P}(o\text{-Tol})_3$) (6.08 mg) were dissolved in anhydrous toluene (12 mL) under nitrogen atmosphere. The reaction mixture was heated at 100 °C with vigorous stirring for 24 h. Then, the trimethylstannyl-terminal groups were capped with 2-bromothiophene (0.05 mL) by refluxing for 1 h. After that, the bromo-terminal groups were capped with 2-(tributylstannyl)thiophene (0.1 mL)

by refluxing for another 1 h. After cooling to room temperature, the polymer was precipitated by pouring the solution into acetone and was collected by filtration through a 0.45 μ m Teflon filter. Then the polymer was washed in a Soxhlet extractor with acetone, diethyl ether, dichloromethane and chlorobenzene (CB). The CB fraction was purified by passing it though a silica gel column and then precipitated from diethyl ether. Finally, the polymer was obtained by filtration through 0.45 μ m Teflon filter and dried under vacuum at 40 °C for 24 h.

Polymer PBDB-T

Starting with 2,6-bis(trimethyltin)-4,8-bis(5-(2-ethylhexyl)thiophen-2-yl)benzo[1,2-*b*:4,5-*b'*]dithiophene (0.25 mmol, 226.1 mg), 1,3-bis(5-bromothiophen-2-yl)-5,7-bis(2-ethylhexyl)benzo[1,2-*c*:4,5-*c'*]dithiophene-4,8-dione (0.25 mmol, 191.7 mg), Yield: 325.9 mg (78%).

Polymer N2200

Starting with NDIBr₂ (0.25 mmol, 246.3 mg), 2T (0.25 mmol, 123.0 mg), Yield: 291.7 mg (79%).

Polymer PNDI-TF5

Starting with NDIBr₂ (0.25 mmol, 246.3 mg), 2T (0.2375 mmol, 116.8 mg) and TF (0.0125 mmol, 5.6 mg). Yield: 261.8 mg (71%).

Polymer PNDI-TF10

Starting with NDIBr₂ (0.25 mmol, 246.3 mg), 2T (0.225 mmol, 110.7 mg) and TF (0.025 mmol, 11.1 mg). Yield: 272.4 mg (74%).

Polymer PNDI-TF15

Starting with NDIBr₂ (0.25 mmol, 246.3 mg), 2T (0.2125 mmol, 104.5 mg) and TF (0.0375 mmol, 16.7 mg). Yield: 275.6 mg (75%).

Table S1. Polymerization yields, number-average (M_n), weight-average (M_w) molecular weights and polydispersity indexes (PDI) of the polymers.

polymer	yield (%)	M_n (kDa)	M_w (kDa)	PDI
PBDB-T	78	65.5	150.7	2.3
N2200	79	60.4	151.0	2.5
PNDI-TF5	71	68.5	198.7	2.9
PNDI-TF10	74	73.7	213.7	2.9
PNDI-TF15	75	79.3	245.8	3.1

3. Thermogravimetric analysis (TGA) measurements

Thermogravimetric analysis (TGA) was carried out on a METTLER TOLEDO thermogravimetric analyzer TGA/DSC 3+, from 50 °C to 600 °C at a heating rate of 10 °C /min under N₂ flow.

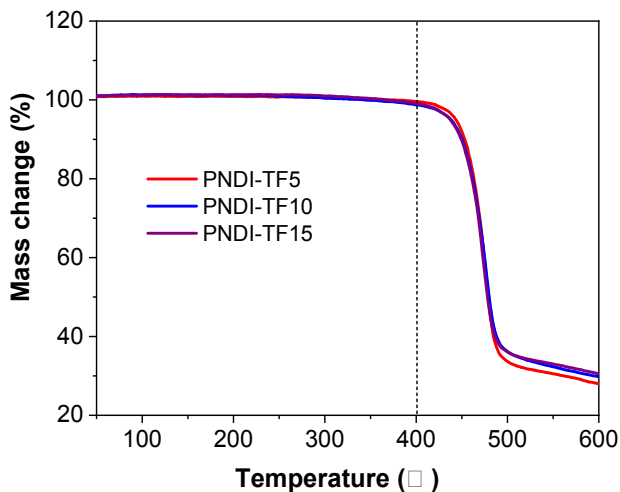


Figure S2. TGA traces of the neat polymers.

4. Optical properties

Absorption spectra was measured with a PerkinElmer Lambda 900 UV–Vis–NIR absorption spectrometer.

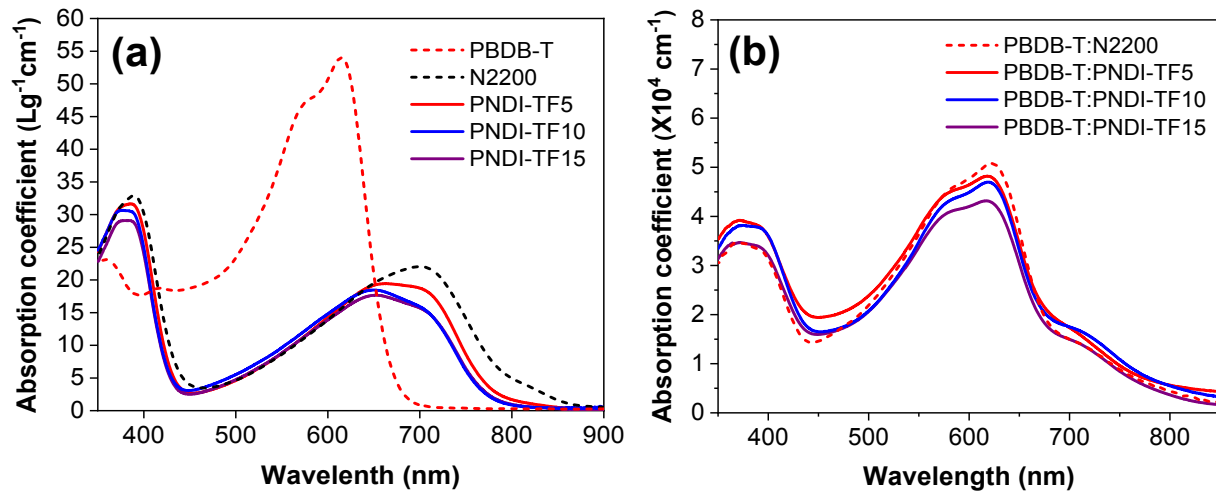


Figure S3. (a) Absorption coefficients of the polymers in CB; (b) Absorption coefficients of the blend films (donor:acceptor = 1:1).

5. Electrochemical properties

Square wave voltammetry (SWV) measurements were carried out on a CH-Instruments 650A Electrochemical Workstation. A three-electrode setup was used with platinum wires for both the working electrode and counter electrode, and Ag/Ag⁺ was used for the reference electrode calibrated with a ferrocene/ferrocenyl couple (Fc/Fc⁺). A 0.1 M nitrogen-saturated solution of tetrabutylammonium hexafluorophosphate (Bu₄NPF₆) in anhydrous acetonitrile was used as the supporting electrolyte. The polymer films were deposited onto the working electrode from the CB solutions.

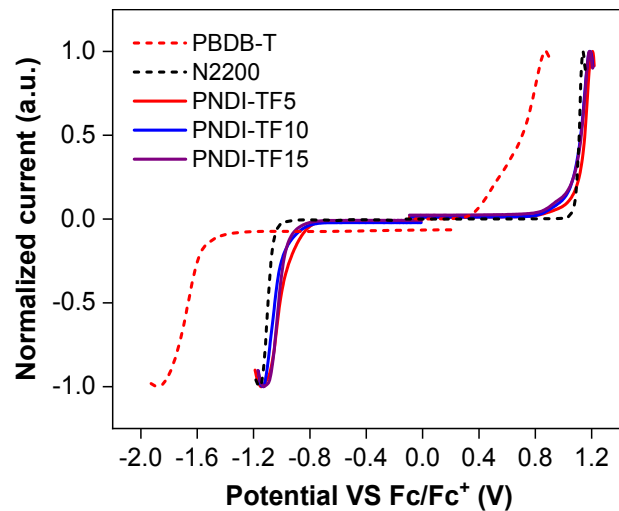
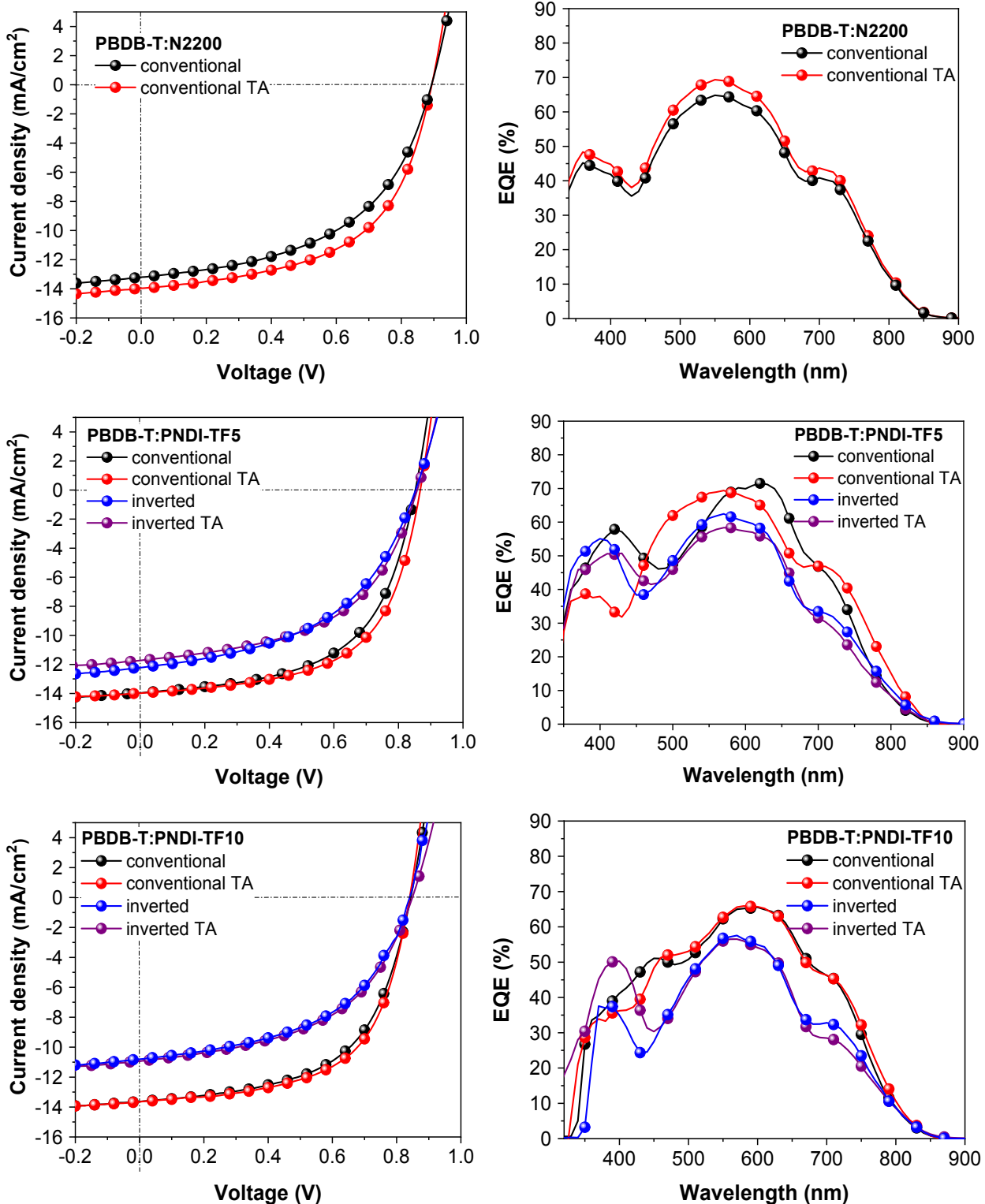


Figure S4. Square wave voltammetry measurements of the polymers.

The HOMO and LUMO levels were estimated from the peak potentials by setting the oxidative peak potential of Fc/Fc⁺ vs. the normal hydrogen electrode (NHE) to 0.63 V, and the NHE vs. the vacuum level to 4.5 V.⁸ The energy levels were calculated according to the formula HOMO = $-(E_{\text{onset,ox vs. Fc/Fc}^+} + 5.13) \text{ eV}$ and LUMO = $-(E_{\text{onset,red vs. Fc/Fc}^+} + 5.13) \text{ eV}$, where the E_{ox} and E_{red} were determined from the onsets of the oxidation and reduction peaks, respectively.

6. J - V and EQE characteristics of the conventional and inverted all-PSCs



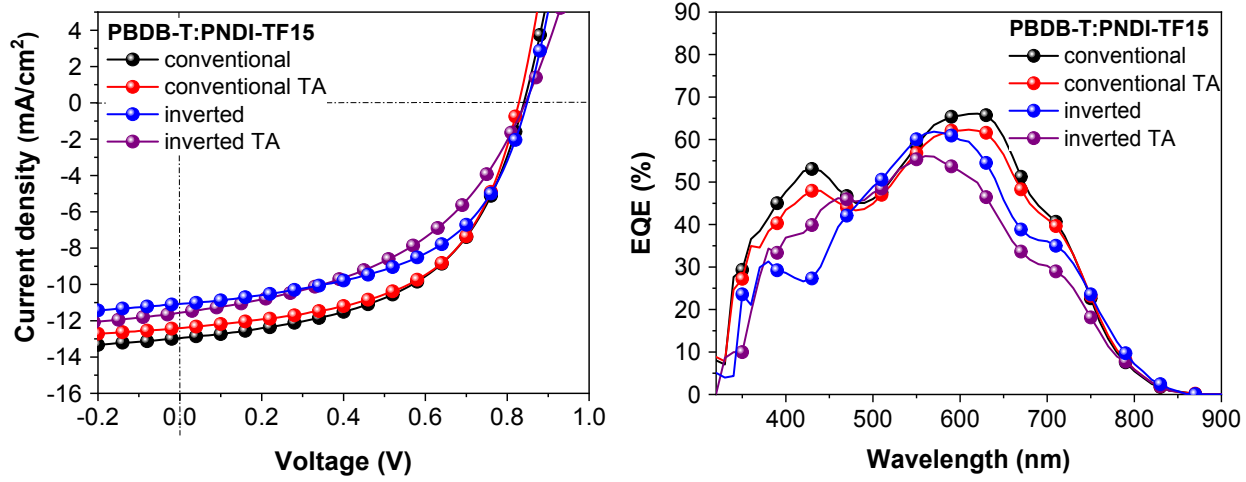


Figure S5. J - V characteristics and the corresponding EQE spectra of the all-PSCs.

Table S2. Photovoltaic parameters data of the all-PSCs based on PBDB-T:acceptor (1: 1, w/w) under the illumination of AM 1.5G, 100 mW cm^{-2} (device area is 0.1 cm^2).

all-PSCs	device structure	condition	V_{oc} (V)	J_{sc} (mA/cm^2)	FF	PCE (%)
PBDB-T:PNDI-TF5	conventional	–	0.86	13.97 (13.61) ^b	0.59	7.1 ^c (7.06±0.04) ^d
		TA ^a	0.87	13.99 (13.66)	0.60	7.3 (7.19±0.11)
	inverted	–	0.85	12.20 (11.85)	0.49	5.1 (5.06±0.04)
		TA ^a	0.85	11.73 (11.33)	0.52	5.2 (5.17±0.03)
	conventional	–	0.84	13.60 (13.01)	0.57	6.6 (6.47±0.13)
		TA ^a	0.84	13.63 (13.10)	0.60	6.9 (6.70±0.20)
PBDB-T:PNDI-TF10	inverted	–	0.84	10.79 (10.23)	0.51	4.6 (4.45±0.15)
		TA ^a	0.84	10.92 (10.40)	0.51	4.7 (4.60±0.10)
	conventional	–	0.84	12.93 (12.54)	0.53	5.8 (5.72±0.08)
		TA ^a	0.83	12.37 (11.97)	0.56	5.7 (5.64±0.06)
PBDB-T:PNDI-TF15	inverted	–	0.85	11.05 (10.24)	0.53	5.0 (4.84±0.16)
		TA ^a	0.84	11.56 (11.05)	0.46	4.5 (4.37±0.13)

^aThermal annealing at 110 °C for 10 min; ^b Photocurrent density obtained by integrating the EQE with the AM1.5G spectrum are given in the parentheses; ^cThe maximal PCE; ^dThe average PCE from fifteen solar cells.

7. $J-V$ and EQE characteristics of the all-PSCs with different D:A ratio

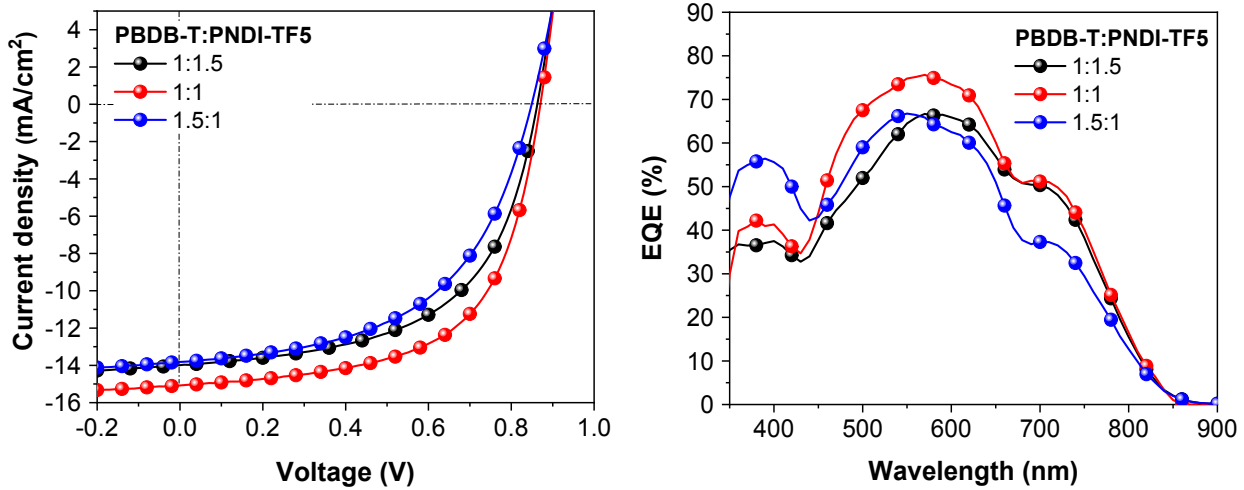


Figure S6. $J-V$ characteristics and the corresponding EQE spectra of the PBDB-T:PNDI-TF5 all-PSCs with different D:A ratio

Table S3. Device parameters of the conventional PBDB-T:PNDI-TF5 all-PSCs with different D:A ratio (active area:0.07 cm²).

D:A ratio	V_{oc} (V)	J_{sc} (mA/cm ²)	FF	PCE (%)
1:1.5	0.86	13.98 (13.49) ^a	0.57	6.9 ^b (6.80±0.10) ^c
1:1	0.87	15.08 (14.89)	0.61	8.0 (7.84±0.16)
1.5:1	0.85	13.82 (13.08)	0.53	6.2 (6.08±0.12)

^a Photocurrent density obtained by integrating the EQE with the AM1.5G spectrum are given in the parentheses; ^b The maximal PCE; ^c The average PCE from fifteen solar cells.

8. J - V characteristics of the all-PSCs with different thermal annealing

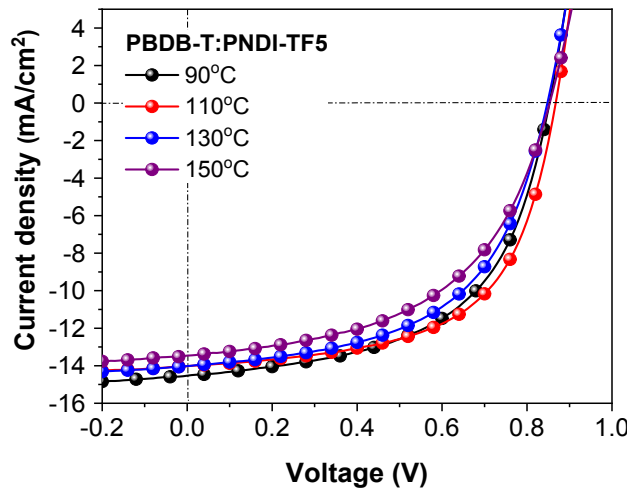


Figure S7. J - V characteristics of the conventional PBDB-T:PNDI-TF5 all-PSCs with different annealing temperature (active area: 0.1cm²).

Table S4. Device parameters of the conventional PBDB-T:PNDI-TF5 all-PSCs with different annealing temperature (active area: 0.1cm²).

temperature (°C)	V_{oc} (V)	J_{sc} (mA/cm ²)	FF	PCE (%)
90	0.85	14.49	0.56	6.9 ^a (6.74±0.16) ^b
110	0.87	13.99	0.60	7.3 (7.19±0.11)
130	0.85	13.98	0.55	6.5 (6.28±0.22)
150	0.85	13.42	0.52	5.9 (5.72±0.18)

^aThe maximal PCE; ^bThe average PCE from fifteen solar cells.

9. J - V characteristics of the all-PSCs with different solvent additives

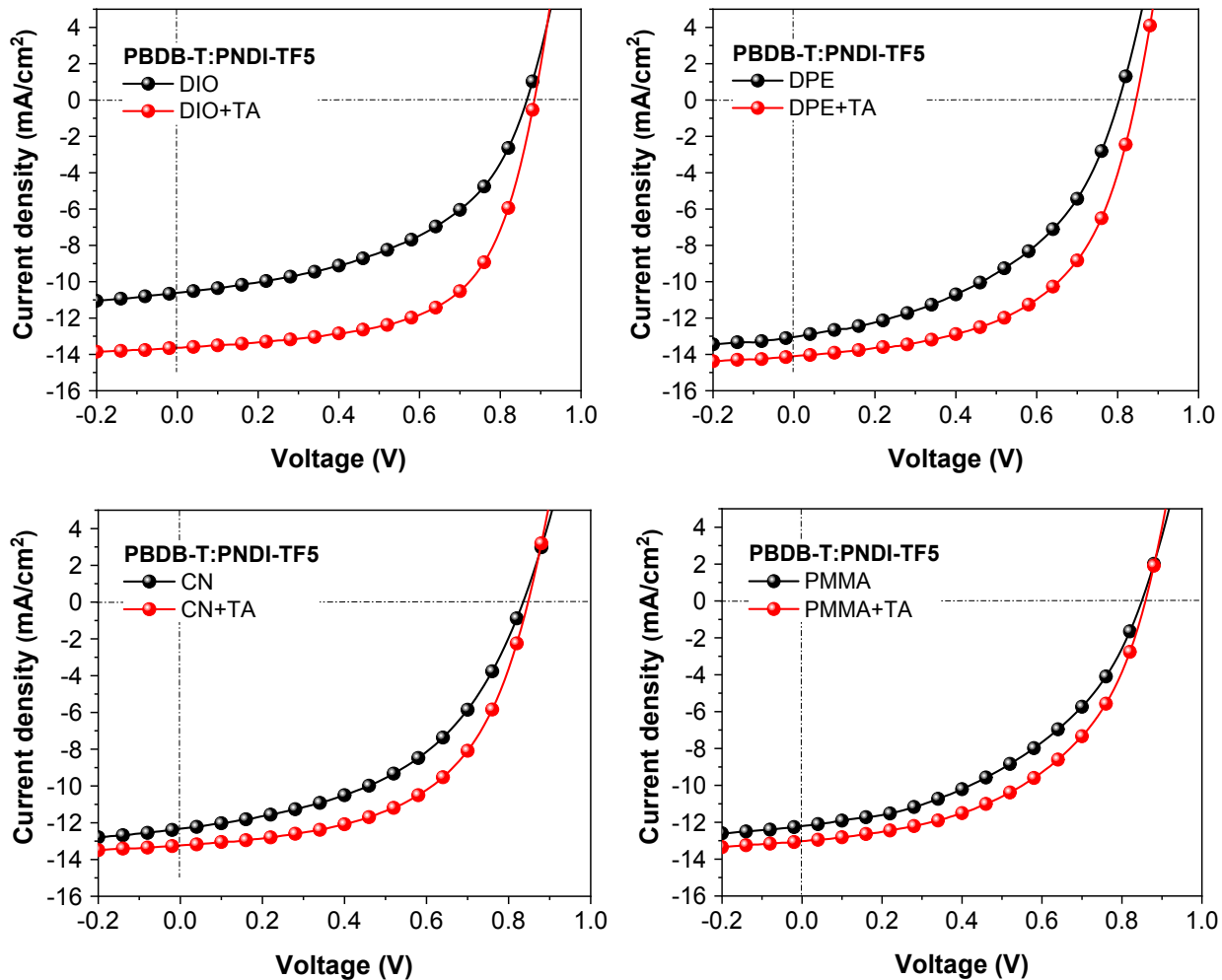


Figure S8. J - V characteristics of the conventional PBDB-T:PNDI-TF5 all-PSCs with different additive treatments (active area: 0.07 cm^2).

Table S5. Device parameters of the conventional PBDB-T:PNDI-TF5 all-PSCs with different additive treatments (active area: 0.07 cm²).

condition	V_{oc} (V)	J_{sc} (mA/cm ²)	FF	PCE (%)
DIO	0.86	10.61	0.49	4.5 ^b (4.35±0.15) ^c
DIO and TA ^a	0.89	13.63	0.61	7.4 (7.27±0.13)
DPE	0.80	13.04	0.46	4.9 (4.65±0.25)
DPE and TA ^a	0.84	14.10	0.56	6.6 (6.49±0.11)
CN	0.84	12.32	0.48	5.0 (4.72±0.28)
CN and TA ^a	0.85	13.23	0.55	6.2 (6.08±0.12)
PMMA	0.85	12.19	0.45	4.7 (4.60±0.10)
PMMA and TA ^a	0.86	12.98	0.50	5.6 (5.34±0.16)

^a Thermal annealing at 110 °C for 10 min; ^b The maximal PCE; ^c The average PCE from fifteen solar cells.

10. J - V characteristics of the all-PSCs with different active areas

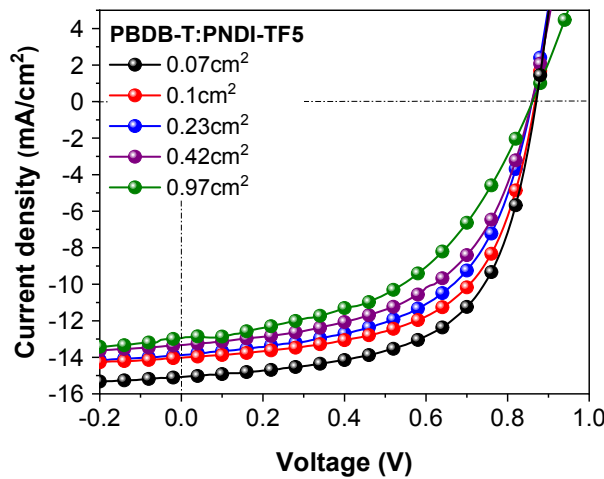


Figure S9. J - V characteristics of the PBDB-T:PNDI-TF5 all-PSCs with different device area.

Table S6. Device parameters of the all-PSCs with different device area.

device area (cm ²)	V_{oc} (V)	J_{sc} (mA/cm ²)	FF	PCE (%)
0.07	0.87	15.08	0.61	8.0 ^a (7.94±0.06) ^b
0.1	0.87	13.99	0.60	7.3 (7.19±0.11)
0.23	0.86	13.88	0.57	6.8 (6.62±0.18)
0.42	0.86	13.29	0.54	6.2 (6.12±0.08)
0.97	0.86	12.95	0.49	5.5 (5.38±0.12)

^a The maximal PCE; ^b The average PCE from fifteen devices.

11. J - V and EQE characteristics of the thick-film all-PSCs

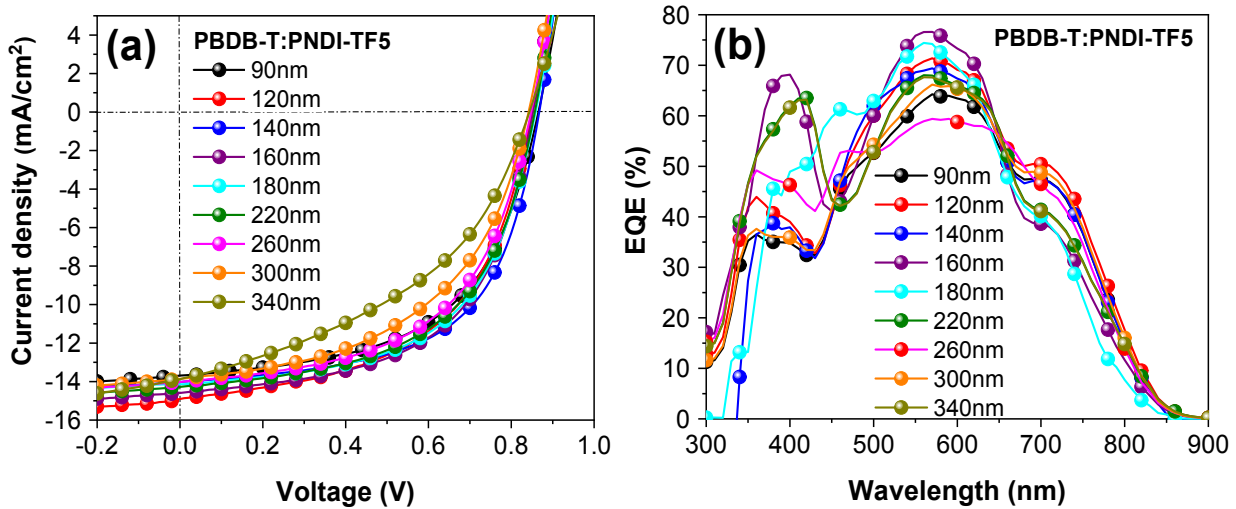


Figure S10. (a) Current density–voltage (J – V) characteristics; (b) EQE curves of the thick film PBDB-T:PNDI-TF5 all-PSCs.

Table S7. Device parameters of the optimal PBDB-T:PNDI-TF5 all-PSCs with different active layer thickness (active area: 0.1 cm^2).

active layer Thickness (nm)	V_{oc} (V)	J_{sc} (mA/cm^2)	FF	PCE (%)
90	0.86	13.67 (13.12) ^a	0.56	6.6 ^b (6.43±0.17) ^c
120	0.85	14.88 (14.34)	0.54	6.8 (6.66±0.14)
140	0.87	13.99 (13.66)	0.60	7.3 (7.19±0.11)
160	0.85	14.54 (14.09)	0.57	7.1 (6.94±0.16)
180	0.86	14.08 (13.58)	0.58	7.0 (6.70±0.30)
220	0.86	14.23 (13.71)	0.56	6.9 (6.71±0.19)
260	0.85	13.98 (13.21)	0.55	6.5 (6.38±0.12)
300	0.84	13.83 (13.51)	0.51	5.9 (5.77±0.13)
340	0.84	14.01 (13.63)	0.43	5.1 (4.95±0.15)

^aPhotocurrent density obtained by integrating the EQE with the AM1.5G spectrum are given in the parentheses; ^bThe maximal PCE; ^cThe average PCE from fifteen solar cells.

12. Tapping-mode atomic force microscopy (AFM) images

The surface morphology of the blend films were acquired by using tapping-mode atomic force microscopy (AFM, Agilent 5500) with MikroMasch NSC-15 AFM tips and resonant frequencies of 300 kHz.

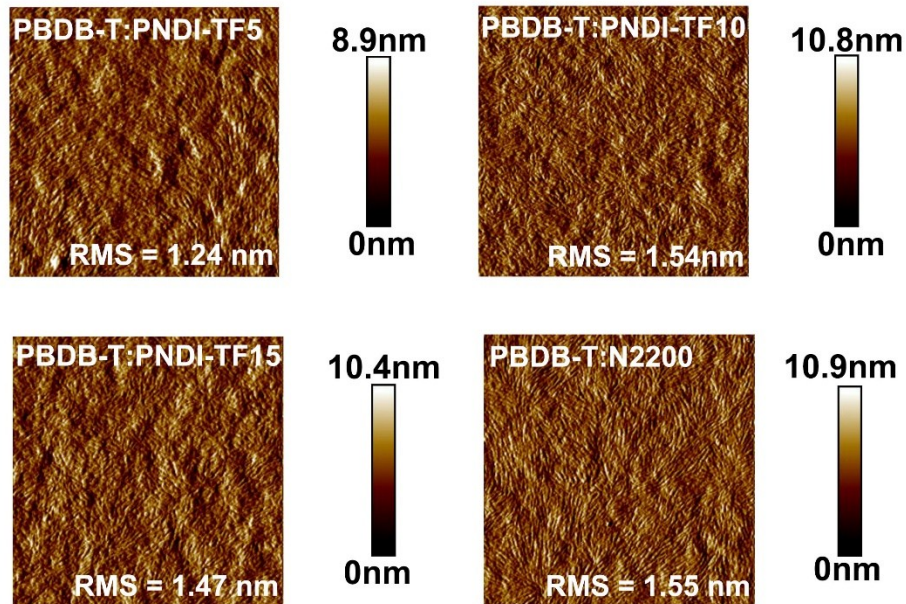


Figure S11. AFM topography ($2.5 \times 2.5 \mu\text{m}^2$) and root-mean-square (RMS) roughness of the blend films.

13. Grazing incidence wide-angle X-ray scattering (GIWAXS) measurements

Table S8. Summary of polymer packing parameters at the in-plane direction

direction	Lamellar stack (100)				
	film	Scattering vector (q) (\AA^{-1})	d -spacing (nm)	FWHM ^a (\AA^{-1})	CL (nm)
in-plane	PBDB-T:N2200	0.267	2.33	0.052	9.81
	PBDB-T:PNDI-TF5	0.268	2.34	0.058	9.77
	PBDB-T:PNDI-TF10	0.269	2.33	0.063	8.98
	PBDB-T:PNDI-TF15	0.267	2.35	0.083	6.85

^aFWHM is full width at half maximum of the scattering peak.

Table S9. Summary of polymer packing parameters in the out-of-plane direction

Direction	π - π stack (010)				
	Blend	Scattering vector (q) (\AA^{-1})	d -spacing (nm)	FWHM ^a (\AA^{-1})	CL (nm)
Out-of-plane	PBDB-T:N2200	1.65	0.37	0.311	1.78
	PBDB-T:PNDI-TF5	1.65	0.38	0.319	1.77
	PBDB-T:PNDI-TF10	1.61	0.39	0.324	1.75
	PBDB-T:PNDI-TF15	1.61	0.39	0.387	1.46

^aFWHM is full width at half maximum of the scattering peak.

14. Relative dielectric constants measurements

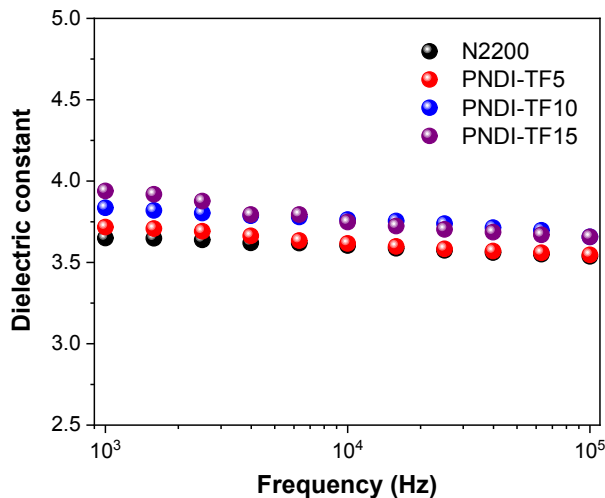


Figure S12. Relative dielectric constants *versus* frequency for the neat acceptor polymers.

15. Time resolved photoluminescence (TRPL) measurements

A Ti:Sapphire laser (Spectra-Physics, Tsunami) at 800 nm and repetition rate 81 MHz with pulse duration of 100 fs was used as an excitation source. Frequency-doubled light (400 nm, generated by Photop Technologies, Tripler TP-2000B) was used for excitation. PL was collected by using two 1 in. quartz plano-convex lenses of 50 mm focal length and focused on the input slit of a spectrograph (Chromex). The output of the spectrograph was sent into the streak camera (Hamamatsu C6860) with a slit width of 20 μm . After background correction of the measured PL images, the shading and spectral sensitivity correction of the fluorescence spectrometer was performed by using calibrated reference light source (Ocean Optics, LS-1-CAL). All samples were kept in N_2 atmosphere, and were measured at room temperature. Efforts were taken to keep the alignment of the experimental set-ups the same for all the samples studied.

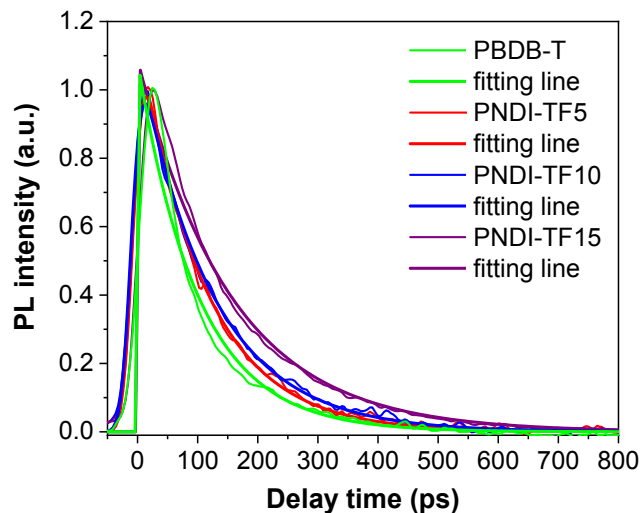


Figure S13. The normalized TRPL kinetics of the neat polymers

Table S10. Parameters of TRPL Measurements^a

polymer	A_1	τ_1 (ps)	A_2	τ_2 (ps)	$\bar{\tau}$ ^b
PBDB-T	1.09	100.2	–	–	–
PNDI-TF5	1.26	108.6	–	–	–
PNDI-TF10	1.21	121.4	–	–	–
PNDI-TF15	1.08	153.7	–	–	–
PBDB-T:PNDI-TF5 (660-680 nm)	2.57	1.3	0.49	7.0	2.2
PBDB-T:PNDI-TF10 (660-680 nm)	1.53	2.6	0.44	13.7	5.1
PBDB-T:PNDI-TF15 (660-680 nm)	1.21	3.8	0.49	20.	8.5
PBDB-T:PNDI-TF5 (860-880 nm)	1.13	27.6	–	–	27.6
PBDB-T:PNDI-TF10 (860-880 nm)	1.01	33.1	–	–	33.1
PBDB-T:PNDI-TF15 (860-880 nm)	0.93	37.5	–	–	37.5

^a Fitting equation: $y = A_1 \exp(-t/\tau_1) + A_2 \exp(-t/\tau_2)$; τ_1 is PL lifetime of PBDB-T in the pure film or

$$\bar{\tau} = \frac{A_1\tau_1 + A_2\tau_2}{A_1 + A_2}$$

blends, τ_2 is PL lifetime of acceptors in pure films or in the blends. ^b

16. Space charge limited current (SCLC) mobility measurements

Hole mobility was measured in a hole-only device composed of ITO/PEDOT:PSS/active layer/MoO₃/Ag. The electron mobility was measured in an electron-only device composed of ITO/ZnO/active layer/PDINO/Ag. For the hole-only device, the blend films were spin-coated on ITO substrates covered with 40 nm PEDOT:PSS. The CB solution of the blends was spin-coated at 1800 rpm for 60 s and baked at 110 °C for 10 min in a glove box. After that, MoO₃ (10 nm) and Ag (80 nm) were successively vacuum-deposited on the active layers. For the electron-only device, sol-gel ZnO was spin-coated onto the ITO-coated glass at a spinning rate of 4000 rpm for 40 s, followed by thermal annealing at 150 °C for 20 min. The CB solution of the blends were spin-coated on the layer of ZnO (40 nm) in a glove box. After that, the ethanol solution of PDINO was spin-coated at 3000 rpm for 25 s. Finally, Ag (80 nm) was vacuum-deposited on top of the PDINO film (5 nm).

According to the Murgatroyd law and using the Equation (S1) to fit the trap-filled region of the $J-V$ curves from the single carrier devices, SCLC mobilities was calculated in a precise way.⁹

$$J = \frac{9}{8\pi} \epsilon_r \epsilon_0 \mu \frac{(V - V_{bi})^2}{L} \exp \left(\frac{0.89}{\gamma} \sqrt{\frac{V - V_{bi}}{kT}} \right) \quad (\text{S1})$$

where J is the current density, ϵ_r is the relative dielectric constant of the polymer blend ($\epsilon_r = 3.6$), ϵ_0 is the free-space dielectric constant, μ is the temperature-dependent mobilities at zero field, L is the thickness of the active layer, $V - V_{bi}$ is the effective voltage, k is Boltzmann constant, T is the absolute temperature and γ is the field enhancement factor.^[4]

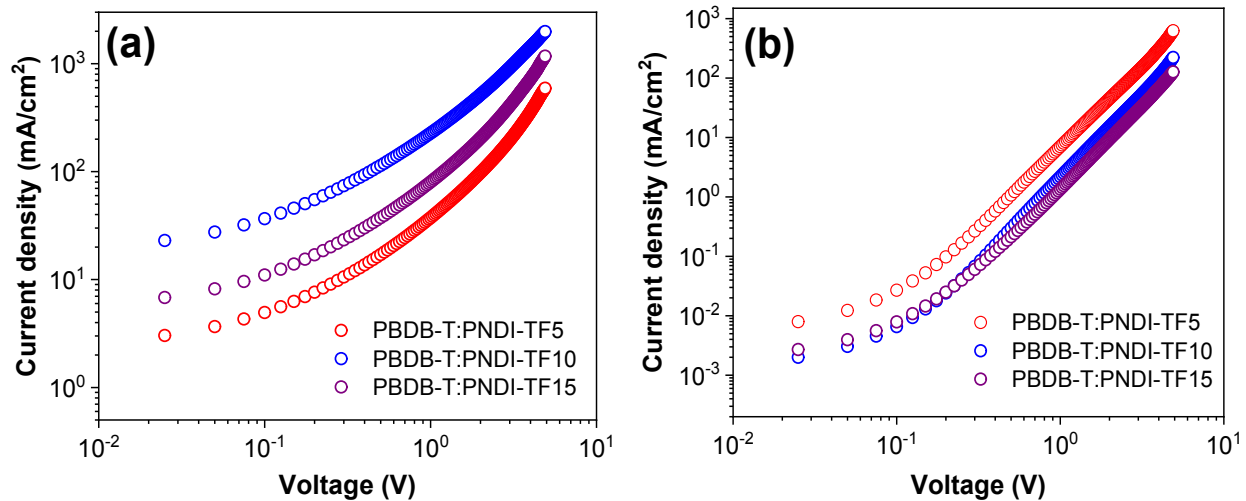


Figure S14. (a) Current density–voltage curves of the blend films with the hole-only device structure of ITO/PEDOT:PSS (40 nm)/active layer/MoO₃(10 nm)/Ag(80 nm). (b) Current density–voltage curves of the blend films with electron-only device structure of ITO/ZnO (40 nm)/active layer/PDINO (5 nm)/Ag (80 nm).

Table S11. Hole and electron mobilities of the all-PSCs.

active layer	condition	μ_h (cm ² V ⁻¹ s ⁻¹)	μ_e (cm ² V ⁻¹ s ⁻¹)	μ_h/μ_e
PBDB-T:PN DI-TF5	TA ^a	2.40×10^{-4}	7.31×10^{-5}	3.3
PBDB-T:PN DI-TF10	TA ^a	1.05×10^{-5}	5.15×10^{-5}	2.0
PBDB-T:PN DI-TF15	TA ^a	8.37×10^{-5}	4.65×10^{-5}	1.8

^a Thermal annealing at 110 °C for 10 min.

17. Recombination characterization

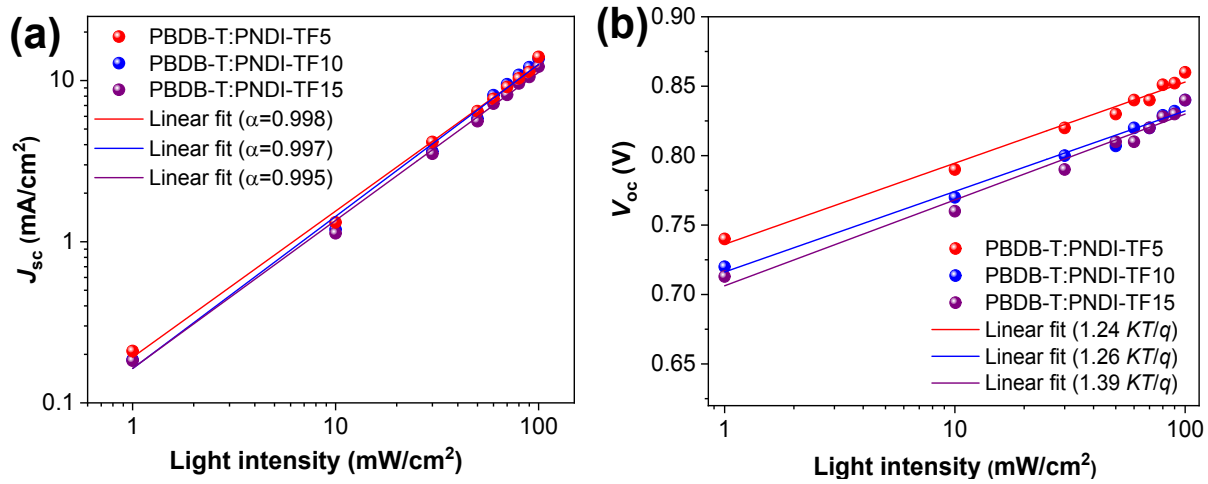


Figure S15. (a) Light intensity dependence of J_{sc} ; (b) light intensity dependence of V_{oc} in the all-PSCs.

18. Thermal stability of the all-PSCs

Table S12. Photovoltaic parameters of thermal stability at 90 °C for the optimized PBDB-T:PNDI-TF5 all-PSCs in a glovebox.

time (h)	V_{oc} (V)	J_{sc} (mA/cm ²)	FF	PCE (%)
0	0.87	14.87	0.58	7.6
0.5	0.87	14.73	0.58	7.5
1	0.87	13.78	0.60	7.3
2	0.86	13.97	0.59	7.1
4	0.86	13.86	0.59	7.0
8	0.86	13.80	0.59	7.0
12	0.86	13.87	0.58	6.9
18	0.86	13.84	0.57	6.9
24	0.86	14.13	0.56	6.8

19. Transmittance of the substrates

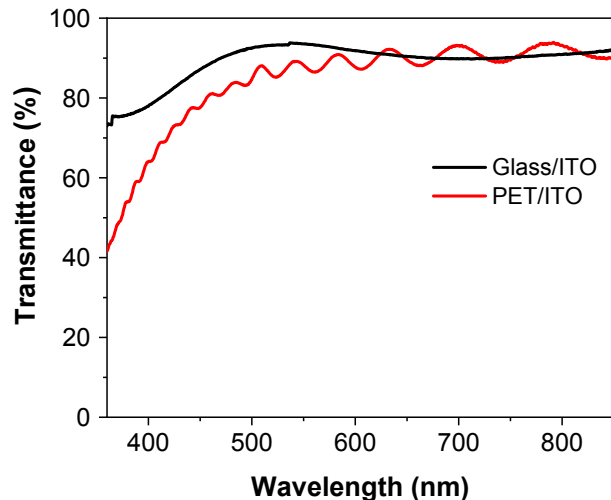


Figure S16. The transmittance of the PET (0.18 mm) /ITO (100 nm) and the glass (0.72 mm) /ITO (130 nm) substrates used in this work.

20. J - V characteristics of the flexible all-PSCs

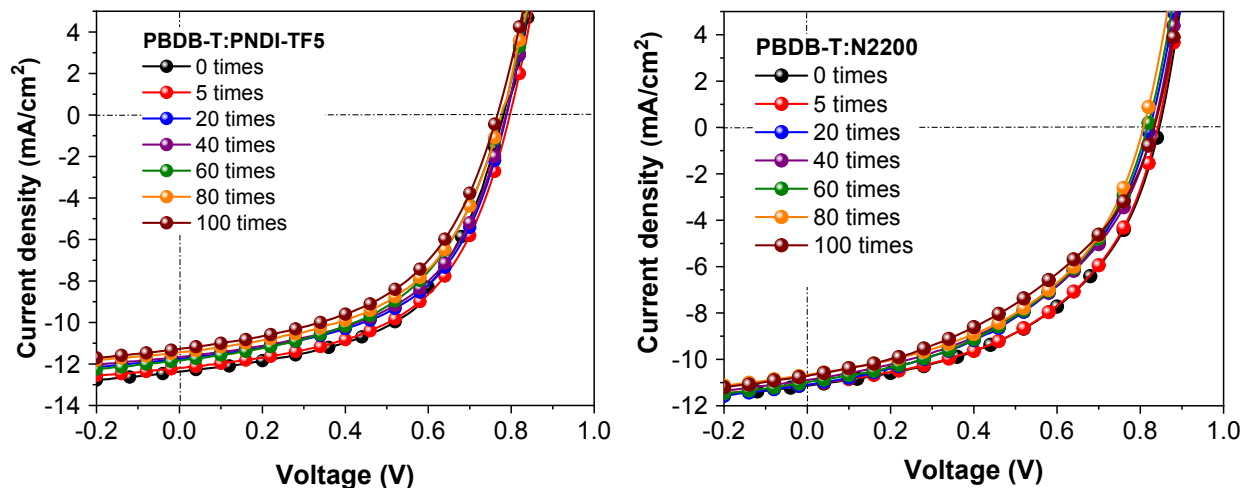


Figure S17. Current density–voltage (J – V) characteristics for the PBDB-T:PNDI-TF5 and PBDB-T:N2200 all-PSCs.

Table S13. Device parameters of the PBDB-T:PNDI-TF5 flexible all-PSCs.

bending cycles (times)	V_{oc} (V)	J_{sc} (mA/cm ²)	FF	PCE (%)
0	0.82	13.12	0.55	5.9
5	0.81	13.21	0.54	5.8
20	0.82	12.40	0.54	5.5
40	0.81	12.30	0.54	5.4
60	0.81	12.09	0.55	5.4
80	0.81	11.98	0.54	5.2
100	0.81	10.86	0.53	4.7

Table S14. Device parameters of the PBDB-T:N2200 flexible all-PSCs.

bending cycles (times)	V_{oc} (V)	J_{sc} (mA/cm ²)	FF	PCE (%)
0	0.84	11.20	0.50	4.7
5	0.84	11.09	0.49	4.6
20	0.82	11.10	0.47	4.3
40	0.83	10.89	0.46	4.2
60	0.82	10.99	0.46	4.1
80	0.81	10.67	0.47	4.1
100	0.83	10.62	0.43	3.8

21. Reference

1. Z. Chen, Y. Zheng, H. Yan and A. Facchetti, *J. Am. Chem. Soc.*, 2009, **131**, 8-9.
2. H. Yan, Z. Chen, Y. Zheng, C. Newman, J. R. Quinn, F. Dotz, M. Kastler and A. Facchetti, *Nature*, 2009, **457**, 679-686.
3. Y. Sakamoto, S. Komatsu and T. Suzuki, *J. Am. Chem. Soc.*, 2001, **123**, 4643-4644.
4. J. Wolf, F. Cruciani, A. El Labban and P. M. Beaujuge, *Chem. Mater.*, 2015, **27**, 4184-4187.
5. D. Qian, L. Ye, M. Zhang, Y. Liang, L. Li, Y. Huang, X. Guo, S. Zhang, Z. a. Tan and J. Hou, *Macromolecules*, 2012, **45**, 9611-9617.
6. Z. Wenchao, Q. Deping, Z. Shaoqing, L. Sunsun, I. Olle, G. Feng and H. Jianhui, *Adv. Mater.*, 2016, **28**, 4734-4739.
7. Z. Li, X. Xu, W. Zhang, X. Meng, W. Ma, A. Yartsev, O. Inganäs, M. R. Andersson, R. A. J. Janssen and E. Wang, *J. Am. Chem. Soc.*, 2016, **138**, 10935-10944.
8. C. M. Cardona, W. Li, A. E. Kaifer, D. Stockdale and G. C. Bazan, *Adv. Mater.*, 2011, **23**, 2367-2371.
9. N. Felekidis, A. Melianas and M. Kemerink, *ACS Appl. Mater. Interfaces*, 2017, **9**, 37070-37077.